Pergamon

Int. J. Solids Structures Vol. 35, Nos 31–32, pp. 4025–4033, 1998

0020–7683/98 $19.00 + .00

PII: S0020–7683(97)00298–9

# FRACTURE MECHANICS MODELING USING IMAGES OF FRACTURE SURFACES

ANNE B. ABELL and DAVID A. LANGE*
Department of Civil Engineering, University of Illinois, 2122 Newmark CE Lab. MC-250, 205 N. Mathews Avenue, Urbana, IL 61801, U.S.A.

(*Received* 1 *November* 1996; *accepted* 16 *May* 1997)

**Abstract**—The fracture surface is important evidence of the behavior of cement-based materials. Deflection, microcracking, and bridging are mechanisms that occur at the crack tip and absorb energy during the fracture process. Two optical microscopy techniques are used in this study to characterize surface geometry. The confocal laser microscope and a video density technique that uses video microscopy provide elevation data for the mesoscale of mortar and concrete. Recently, surface maps have been used to establish a link between surface roughness and fracture. In this paper, the tortuosity of the fracture surface is used in a micromechanical model to predict the increase in toughness due to aggregate. This analysis is performed for two sets of mortar specimens to investigate the influence of the aggregate size and gradation. The influence of crack deflection and aggregate fracture is compared to tested fracture parameters. © 1998 Elsevier Science Ltd. All rights reserved.

## 1. INTRODUCTION

Characterization of fracture surfaces is an area of investigation that provides understanding about the relationship of geometry and microstructure to the mechanical behavior of mortar and concrete. Mechanisms involved in fracture such as microcracking, aggregate deflection, bridging and roughness induced closure are indicated by physical evidence or artifacts during or after the separation of the material with a macrocrack. Images of the surface obtained from scanning electron microscopes (SEM), optical and confocal laser microscopes, and video capture provide qualitative information about the fracture. In addition, the confocal microscope and a video density technique obtain quantitative data of the surface with a topographic map. This data can be analyzed to determine the roughness of the surfaces, and can be used as input for a micromechanical model that predicts the local fracture toughness increase from the crack deflection. Fracture toughness values determined from mechanical testing, resulting in the fractured surfaces, can be compared to the surface parameters.

Confocal microscopy has been used to conveniently obtain elevation data for cement paste and mortar fracture surfaces (Lange *et al.*, 1993). This technique assembles a series of optical sections taken at different focal planes into a digital image where every $x,y$ coordinate (pixel) value is assigned a $z$-level from the section with the brightest value at that location. Figure 1 compares the surface image obtained from an SEM to that reconstructed from a confocal range image for a DSP mortar.

Video microscopy has also been used to image concrete fracture surfaces (Issa *et al.*, 1993). The technique obtains images of the surface covered with varying depths of a colored, non-staining fluid. The gray values in the range image can be calibrated to represent elevation heights. In this study, the technique has been adapted to obtain the surface topology of paste and mortar surfaces. Figure 2 shows a concrete specimen and the corresponding video surface representation.

The topological information provided by both methods can be used to determine the surface area from the geometric construction of triangular planes defined by the $x$-$y$-$z$ coordinates of each pixel. From this area, a surface roughness number (RN) can be found. The coordinates can also be used to determine the crack profile deflection angles.

* Corresponding author.

A model which predicts the fracture toughness increase due to crack deflection around second phase particles in a matrix was proposed by Faber and Evans (1983). Based on the reduction in local stress intensity at the crack tip when it is deflected or when the crack plane is bowed, the model predicted the average strain energy release rate due to particle morphology, aspect ratio, spacing and volume fraction of the second phase. The topographic maps from the image techniques mentioned provide the actual crack tortuosity so that the deflection (tilt) and bowing (twist) angles can be input directly into the model to estimate the fracture toughness increase from that of a flat crack through the plain matrix.

## 2. EXPERIMENTAL PROCEDURE AND TECHNIQUE

The effect of aggregate size and gradation on the material properties and fracture surface geometry of mortars was of interest in this investigation. Mortar, as a simpler composite material (two phases) than concrete, can be modeled directly with the mechanics of materials model. The materials were tested for fracture toughness and the resulting surfaces were imaged.

### 2.1. *Materials*

The materials tested were a mortar of ordinary Portland cement (OPC) with a w/c ratio of 0.45 and 1 : 3 ratio by weight of cement to sand, and an OPC paste of w/c ratio of 0.45. Two sample sets of mortars were designed. The fine aggregate was graded with standard sieve sizes of 9.5 mm, No. 4, 8, 16, 30, 50 and 100 and the distribution in comparison to ASTM C33 limits is presented in Table 1. The maximum aggregate set consisted of four designs which eliminated the particles collected on sieves above the sizes of No. 4, 8, 16 and 30. The mono-sized aggregate set consisted of three designs which used the particles collected on the sieve sizes No. 8, 16 and 30, and the surfaces are shown in Fig. 3 (top). The surfaces for the maximum aggregate set are shown in Fig. 3 (bottom). Silica sand of ASTM grades 20/30, 50/70 and ASTM C190 were used for the gradation from sieves No. 30–50 to reduce the incidence of aggregate fracture. River sand was used for all other sieve sizes.

The mortars and paste were cast into bars of size 38.1 mm (1.5 in.) × 25.4 mm (1 in.) × 177.8 mm (7 in.) with a notch of 12.7 mm (0.5 in.) in height at mid-span. Four bars were cast of each mix. The bars were moist cured for 28 days prior to testing.

### 2.2. *Testing*

Three-point bend tests were performed on the specimens following the Two-Parameter Fracture Model method [RILEM, 1990]. The loading span was 152.4 mm (6 in.). The critical stress intensity factor, $K_{IC}$, and Young's Modulus determined from the tests and averaged over the sample set are shown in Table 2. The average of $K_{IC}$ for the Max4 sample set was lower than that for the Max8 sample set due to heterogeneity within the set.

Table 1. Fine aggregate base grading

| Sieve size | Cumulative % passing (wt.) | ASTM C33 limits |
|---|---|---|
| 9.5 mm | 100 | 100 |
| No. 4 | 94 | 95–100 |
| No. 8 | 81 | 80–100 |
| No. 16 | 68 | 50–85 |
| No. 30 | 37 | 25–60 |
| No. 50 | 12 | 10–30 |
| No. 100 | 0 | 2–10 |

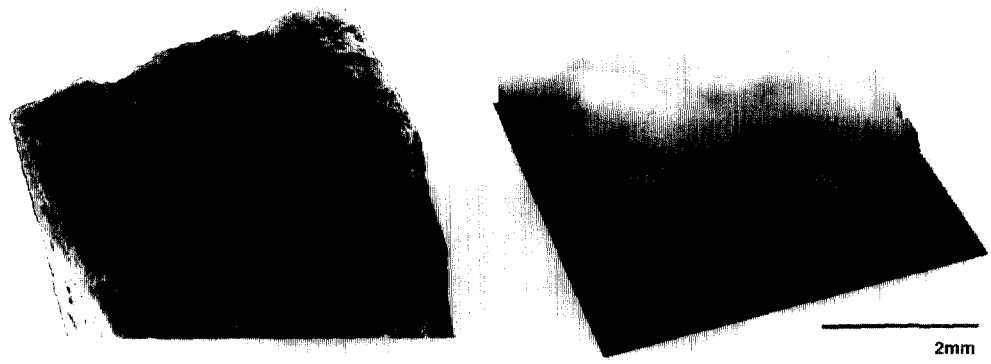


Fig. 1. SEM micrograph compared to confocal range image for mortar fracture surface.

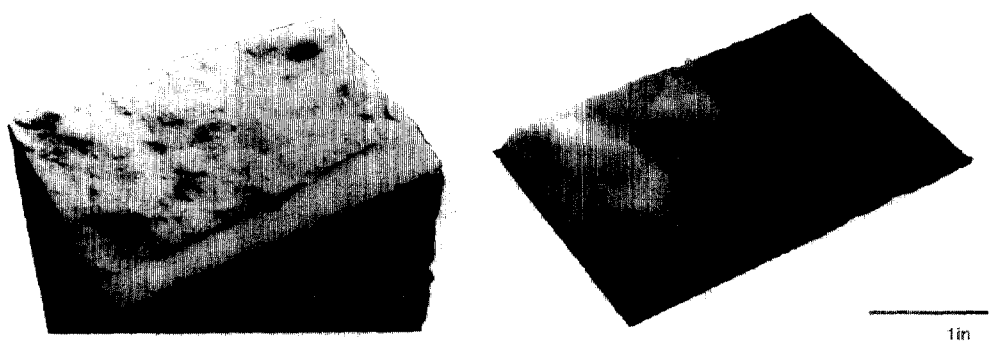


Fig. 2. Photograph compared to video density range image for a concrete fracture surface.

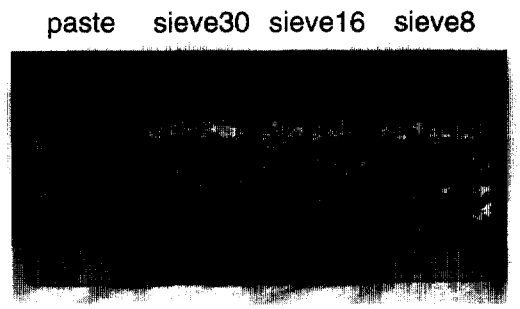


Fig. 3. Fracture surfaces of specimens.

Table 2. Material properties of specimens

| Specimen set | $E$ (MPa) | $K_{IC}$ (N/m$^{3/2}$) |
|---|---|---|
| Paste | 3.24E+04 | 2.35E+05 |
| Sieve8 | 5.38E+04 | 5.73E+05 |
| Sieve16 | 4.96E+04 | 5.47E+05 |
| Sieve30 | 8.00E+04 | 4.95E+04 |
| Max4 | 5.60E+04 | 5.68E+05 |
| Max8 | 5.93E+04 | 5.77E+05 |
| Max16 | 6.81E+04 | 5.26E+05 |
| Max30 | 6.46E+04 | 4.80E+05 |

### 2.3. *Image acquisition*

2.3.1. *Confocal microscopy.* Images were acquired with a confocal laser-scanning microscope with a 2.5X lens at a magnification of 20 to produce a field size of approximately 3.5 mm × 3.5 mm. The $z$ slice thickness was 18 $\mu$m. Ten images were taken for each specimen in a random grid pattern across the surface. Contrast and brightness were adjusted to maximize the brightness range of 0 to 255. The digital images are 256 × 512 pixels with the top half containing the topographic map and the lower half containing the "through-focus" image which appears as a focused image of the surface. All images were filtered with a median filter to reduce noise. This filter alters the image by replacing each pixel with the median $z$ value from the original image of the pixel and eight surrounding pixels.

2.3.2. *Video density technique.* Images were acquired with a CCD video camera and the public domain NIH Image program (developed at the U.S. National Institute of Health and available on the Internet at http://rsb.info.nih.gov/nih-image/) running on a Macintosh computer. The specimens were coated with a flat white opaque paint to eliminate color variations within the paste and aggregate. The specimens were submerged in a purple water solution to cover the peak elevation. The surface was captured as an image file by averaging eight frames, and obtaining eight sections corresponding to approximately 3 mm × 3 mm. The gray scale values were calibrated to the surface elevation.

## 3. ANALYSIS AND DISCUSSION

### 3.1. *Image analysis*

A common parameter to describe the geometry of a surface is the roughness number (RN). This value quantifies the relation of the measured surface area to the nominal area if the surface was planar. For example, the ratio of the area of a flat surface to the nominal area would be an RN value of 1.0. In order to determine the surface area from the topographic maps, triangles are constructed between pixels, and the area is summed over all the triangles (Lange *et al.*, 1993). Roughness values are related to the scale at which the surface is investigated. The roughness values from the confocal and video density techniques are presented in Table 3.

Table 3. Roughness numbers

| Specimen set | Confocal | Video density |
|---|---|---|
| Paste | 1.9260 | 1.6320 |
| Sieve8 | 2.3071 | 2.3485 |
| Sieve16 | 2.3188 | 2.4874 |
| Sieve30 | 2.7698 | 3.0623 |
| Max4 | 2.4758 | 2.7841 |
| Max8 | 2.5324 | 2.9988 |
| Max16 | 2.5428 | 3.2053 |
| Max30 | 2.5663 | 3.1313 |

3.2. *Micromechanical model*

The topological surface data is also useful for examining the effect of the tortuosity of the crack on the energy required to create the surface. A micromechanical model based on the reduction in the local stress intensity factor at an aggregate when the crack path is deflected or the crack front is bowed by an inclusion in a matrix can predict the increase in toughness from the matrix toughness for a planar crack (Faber and Evans, 1983).

The fracture mechanics model applied to the confocal microscope image data calculates an average strain energy release rate from the tilted and twisted portions of the crack front. The crack front is deflected by inclusions out of plane by a tilt angle, $\theta$, and the crack projection is bowed around the inclusions by a twist angle, $\phi$, as shown in Fig. 4. The tilted crack has Mode I (opening) and Mode II (sliding) contributions to the local stress intensity; while the twisted crack has Mode I and Mode III (tearing) contributions.

The strain energy release rate, $G$, and the local stress intensity factors, $k_1'$ and $k_2'$, for a tilted segment of crack are determined by (Faber and Evans, 1983)

$$EG = k_1'^2(1-\nu^2)+k_2'^2(1-\nu^2) \tag{1}$$

$$k_1' = \cos^3(\theta/2)K_I \tag{2a}$$

$$k_2' = \sin(\theta/2)\cos^2(\theta/2)K_I \tag{2b}$$

where $E$ and $\nu$ are the Young's modulus and Poisson's ratio of the material, respectively. The strain energy release rate and the local stress intensity factors, $k_1^T$ and $k_3^T$, for a twisted segment of crack are determined by (Faber and Evans, 1983)

$$EG = k_1^{T2}(1-\nu^2)+k_3^{T2}(1+\nu) \tag{3}$$

$$k_1^T = \cos^4(\theta/2)[2\nu\sin^2\phi+\cos^2(\theta/2)\cos^2\phi]k_1' + \sin^2(\theta/2)\cos^2(\theta/2)[2\nu\sin^2\phi+3\cos^2(\theta/2)\cos^2\phi]k_2' \tag{4a}$$

$$k_3^T = \cos^4(\theta/2)[\sin\phi\cos\phi(\cos^2(\theta/2)-2\nu)]k_1' + \sin^2(\theta/2)\cos^2(\theta/2)[\sin\phi\cos\phi(3\cos^2(\theta/2)-2\nu)]k_2' \tag{4b}$$

where the angular functions are determined by resolving the normal and shear stresses of the tilted crack onto the twist plane.

The local crack path angles were determined for each segment from the difference in $z$ elevations and horizontal distance between adjacent pixels. Figure 5 shows the surface representation and the local angles. The toughening ratio of the deflected toughness to the undeflected toughness was determined by

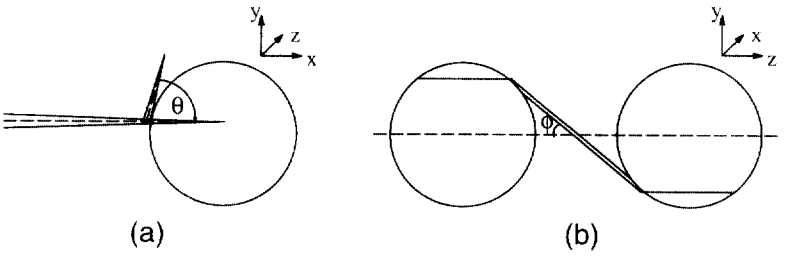


Fig. 4. Deflection at the crack tip: (a) tilt and (b) twist.

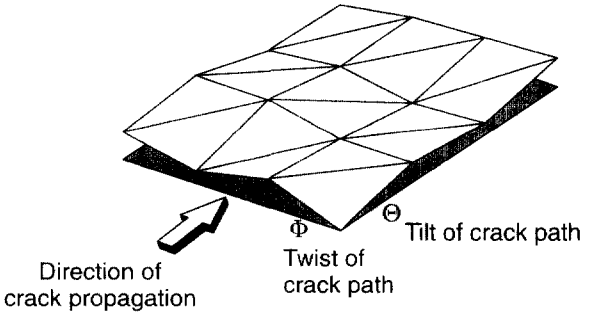


Fig. 5. Range image of fracture surface for micromechanical model.

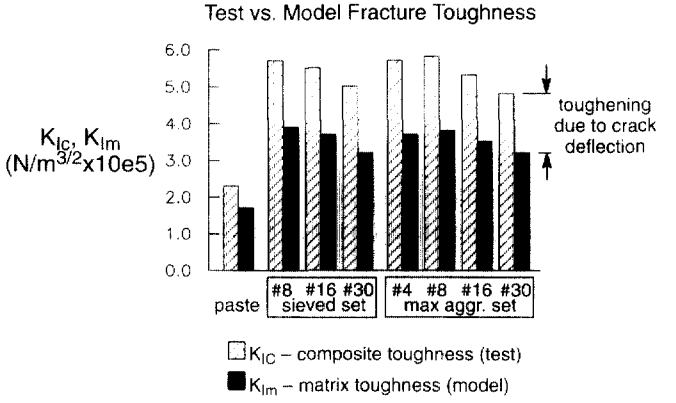


Fig. 6. Fracture toughness from model compared to test results.

$$\text{Toughening ratio} = \frac{K_I}{\sqrt{\text{average } EG}} \tag{5}$$

where $K_I$ is set equal to 1.0 and $EG$ is calculated from eqns 1–4. The model predicts an increase in the toughness from the undeflected matrix for the composite. Figure 6 shows the relationship between the mortar specimens with single sieve aggregate distributions, those with the same gradation but different maximum aggregate, and the cement paste specimen. The addition of the aggregate in the matrix results in an increase in the matrix toughness which has also been reported for fiber reinforced materials (Lange *et al.*, 1994). The difference between the undeflected crack toughness of cement paste to that of the mortars can be explained by the presence of other mechanisms besides crack deflection. Aggregate interlock, microcracking under the exposed surfaces, and the effect of elasticity mismatch between aggregate and matrix in the interfacial zone are mechanisms that are not accounted for in the model.

### 3.3. *Interpretation of results*

The roughness values for the two techniques as presented in Table 3 show good agreement. The values for the mortars are consistently higher and show the same increasing trend with aggregate size. The differences between RN measured between the two techniques arise from the application of lighting in the techniques. Confocal microscopy uses a focused laser light to determine the brightness at a single data point or pixel, whereas the lighting for video density microscopy illuminates the entire submerged surface which is then recorded. Artifacts from the general lighting in the video microscopy technique such as shadowing and glare can influence the surface elevation measurement.

The roughness values of the specimen set were also compared with the ratio of the toughness of the composite material to that of the undeflected toughness determined by the

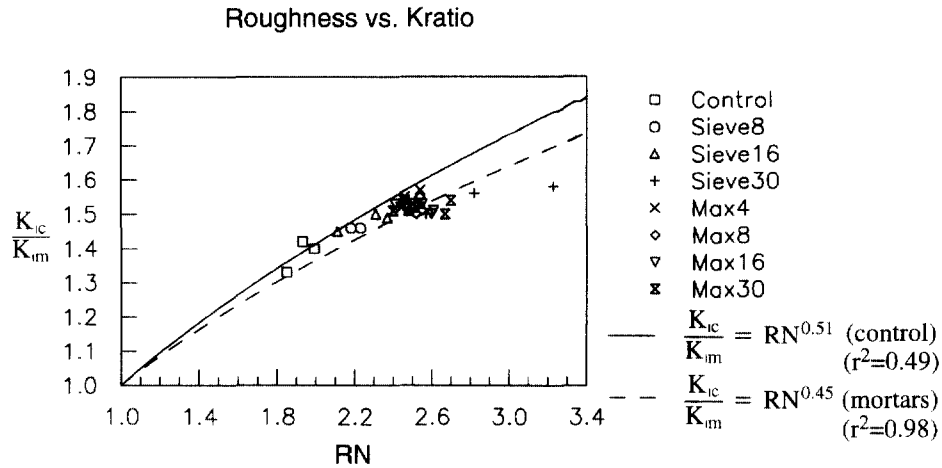


Fig. 7. Relation between fracture surface roughness and fracture toughness.

model as shown in Fig. 7. The relationship for a linear-elastic material where all the energy in fracture goes into creating the surfaces is described by eqn 6 and shown in Fig. 7 (Xin *et al.*, 1995):

$$\frac{K_{IC}}{K_{Im}} = \sqrt{RN} \tag{6}$$

The cement paste exhibited the lowest RN values and more closely behaved as a linear-elastic material. The mortars exhibited higher RN values, and showed greater deviation from eqn 6 at the highest RN values. This result suggests that greater roughness in the crack path implies higher toughening through crack deflection, but also indicates increasing significance of other energy absorbing mechanisms.

The RN parameters and the toughening increases predicted by the model show the degree of variation for paste and mortar from linear-elastic behavior. The presence of sand in mortar tends to permit the crack path to become dominated by grain shape as the crack path weaves its way around the inclusions. Cracks in pastes with no inclusions (at the size scale of millimeters) can more freely propagate before arrest.

## 4. SUMMARY

From the investigation of fracture surface geometry, the mechanical behavior of mortars can be better understood. The mechanisms involved in the process such as crack deflection, can be recorded through confocal and video microscopy range images. Through image analysis, parameters such as roughness can be obtained and compared to the material toughness. Also, the surface information can be input into a micromechanical model to determine the fracture toughness increase due to the inclusion of aggregate in a matrix. The model was applied to topology data for cement paste and mortar samples of differing aggregate sizes and maximum aggregate sizes. The model showed that crack deflection is a major source of toughening, but the model did not fully reconcile the toughness of paste and mortars. Thus, the results suggest that other mechanisms in addition to crack deflection contribute to the energy of fracture. The relation of the toughening ratio to the roughness value illustrates the difference in material behavior when aggregate is added to cement paste, and shows how the fracture behavior of cement-based materials increasingly deviates from linear elastic as fracture surface roughness increases.

*Acknowledgment*—This research was supported by the NSF Center for Advanced Cement-Based Materials (NSF Grant No. DMR 88808423-01).

## REFERENCES

Abell, A. B. and Lange, D. A. (1994) Image-based characterization of fracture surface roughness. *Mat. Res. Soc. Symp. Proc.* **370,** 107–113.

Faber, K. T. and Evans, A. G. (1983) Crack deflection processes—I. Theory. *Acta Metall.* **31**(4), 565–576.

Issa, M. A., Hammad, A. M. and Chudnovsky, A. (1993) Correlation between crack tortuosity and fracture toughness in cementitious material. *International Journal of Fracture* **60,** 97–105.

Lange, D. A., Jennings, H. M. and Shah, S. P. (1993) Analysis of surface roughness using confocal microscopy. *Journal of Materials Science* **28,** 3879–3884.

Lange, D. A., Sun, G. K. and Bloom, R. (1994) Fracture of microfiber reinforced DSP materials. *Cement Transactions (Amer. Ceramic Society)* **40,** 239–246.

RILEM Draft Recommendations, TC89-FMT Fracture Mechanics of Concrete—Test Methods (1990) Determination of Fracture Parameters ($K_{Ic}^{s}$ and $CTOD_c$) of Plain Concrete Using Three-Point Bend Tests. *Materials and Structures* **23,** 457–460.

Xin, Y., Hsia, K. J. and Lange, D. A. (1995) Quantitative characterization of the fracture surface of Si single crystals by confocal microscopy. *Journal of the American Ceramic Society* **78,** 3201–3208.